Inorganic Chemistry

Article

pubs.acs.org/IC

Hume–Rothery Phase-Inspired Metal-Rich Molecules: Cluster Expansion of $[Ni(ZnMe)_6(ZnCp^*)_2]$ by Face Capping with $Ni^0(\eta^6$-toluene) and $Ni^I(\eta^5$-Cp*)

Mariusz Molon,[†] Christian Gemel,[†] Paul Jerabek,[‡] Lukas Trombach,[‡] Gernot Frenking,[‡] and Roland A. Fischer*,[†]

[†]Inorganic Chemistry II—Organometallics & Materials, Ruhr-Universität Bochum, D-44780 Bochum, Germany

[‡]Department of Chemistry, Philipps-University Marburg, 35032 Marburg, Germany

Supporting Information

ABSTRACT: The novel all-hydrocarbon ligand-stabilized binuclear clusters of metal–core composition Ni_2Zn_7E, $[(\eta^5\text{-Cp}^*)Ni_2(ZnMe)_6(ZnCp^*)(ECp^*)]$ (**1-Zn**, E = Zn; **1-Ga**, E = Ga) and $[(\eta^6\text{-toluene})Ni_2(ZnCp^*)_2(ZnMe)_6]$ (**2**; Cp* = pentamethylcyclopentadienyl), were obtained via Ga/Zn and Al/Zn exchange reactions using the starting compounds $[Ni_2(ECp^*)_3(\eta^2\text{-}C_2H_4)_2]$ (E = Al/Ga) and an excess of $ZnMe_2$ (Me = CH_3). Compounds **1-Zn** and **1-Ga** are very closely related and differ only by one Zn or Ga atom in the group 12/13 metal shell (Zn/Ga) around the two Ni centers. Accordingly, **1-Zn** is EPR-active and **1-Ga** is EPR-silent. The compounds were derived as a crystalline product mixture. All new compounds were characterized by ^{1}H and ^{13}C NMR and electron paramagnetic resonance (EPR) spectroscopy, mass spectrometric analysis using liquid-injection field desorption ionization, and elemental analysis, and their molecular structures were determined by single-crystal X-ray diffraction studies. In addition, the electronic structure has been investigated by DFT and QTAIM calculations, which suggest that there is a Ni1–Ni2 binding interaction. Similar to Zn-rich intermetallic phases of the Hume–Rothery type, the transition metals (here Ni) are distributed in a matrix of Zn atoms to yield highly Zn-coordinated environments. The organic residues, ancillary ligands (Me, Cp*, and toluene), can be viewed as the "protecting" shell of the 10-metal-atom core structures. The soft and flexible binding properties of Cp* and transferability of Me substituents between groups 12 and 13 are essential for the success of this precedence-less type of cluster formation reaction.

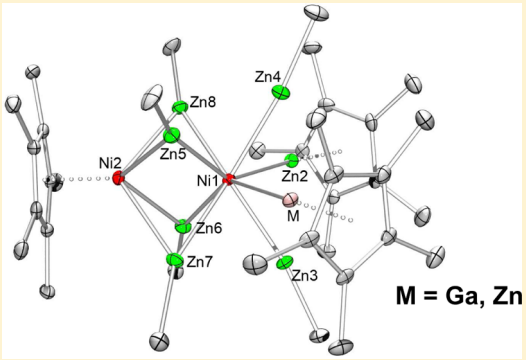

INTRODUCTION

The structural identification of ferrocene $[Fe(\eta^5\text{-}C_5H_5)_2]$[1−4] by Fischer, Wilkinson, and Woodward shattered the young field of organometallic chemistry and led to its rapid growth. Since then, a tremendous amount of neutral and charged complexes, including ansa-bridged and half-sandwich types of compounds, have been studied intensively. Besides them, bis-arene structures like $[Cr(\eta^6\text{-}C_6H_6)_2]$[5] and $[U(\eta^8\text{-}C_8H_8)_2]$[6,7] have been known for decades, but in contrast, zerovalent d^{10} metal(η^6-arene) complexes are still rare, which may arise from the electron-rich situation of the d^{10} metal center, resulting in a low σ-donor/π-acceptor bonding efficiency and, thus, low thermal stability of these moieties. A few examples of such Ni(η^6-arene) complexes that are stable enough to be characterized by single-crystal X-ray analysis have been reported: Mostly, strong σ donors are able to stabilize these highly reactive $Ni^0(\eta^6$-arene) complexes, including N-heterocyclic carbenes (NHCs), ylides like silylene and phosphine, and low-valent Ga^IAr' [Ar′ = C_6H_3-2,6-(C_6H_3-2,6-*i*-Pr_2)$_2$] ligands.[8−12]

In 2004, the first zinc(I) metallocene-like complex, $[Zn_2(\eta^5\text{-}Cp^*)_2]$,[13,14] containing the first stable Zn–Zn bond in a molecular complex was established. This compound turned out to be a good candidate for the facile generation of ZnZnCp* and ZnCp* one-electron donor ligands trapped at d^{10} metals, to form Zn-rich molecules of the type $[M(ZnZnCp^*)_4(ZnCp^*)_4]$[15] (M = Ni, Pd, Pt) and $[Pd(ZnCp^*)_4(ZnMe)_2\{Zn(tmeda)\}]$,[16] among others.[17] Likewise, through selective Ga/Zn exchange reactions and involved redox processes, GaCp*-ligated transition-metal complexes $[M(GaCp^*)_n]$ can be transformed into all-Zn-ligated, pseudohomoleptic, and highly coordinated compounds $[M(ZnR)_{2n}]$[18,19] ($n \geq 4$; M = Mo, Ru, Rh, Ni, Pd, Pt; R = Me, Et, Cp*). The structures of these molecules mimic cutouts of the corresponding intermetallic Zn-rich Hume–Rothery phases, where the transition-metal atoms are imbedded in a matrix of Zn atoms and feature various coordination polyhedra with high coordination numbers, CN ≥ 8. Common alloys such as Cu/

Received: June 23, 2014
Published: September 22, 2014

Zn brass are textbook example of Hume−Rothery phases. For example, the γ-brass phase, Cu_5Zn_8, is structurally (and electronically) similar to the Cu_9Al_4 and Ni_2Zn_{11} phases. The so-called Hume−Rothery rules derived in the 1920s and 1930s provide empirical classifications of preferred compositions and structures, the origin of these rules was rigorously investigated and explained more recently based on first-principles band structure calculations, and Hume−Rothery phase stabilization mechanisms were identified.[20a] We are inspired, on the one hand, by some heuristic connections between structural motifs found in such kinds of solid-state intermetallics and, on the other hand, by molecular coordination and cluster compounds of similar metal combinations and core structures. Thus, we speculated that our molecular chemistry of $[M(ZnR)_{2n}]$ may be systematically expanded to more complex exclusively metal-loligated and possibly even larger aggregates, which feature binuclear or oligonuclear complexes or clusters $[M_a(ER)_b]$ ($a \geq b$; E = group 12/13 metal atom; R = hydrocarbon ligand) with the transition-metal centers M distributed within a matrix of both terminal coordinating and bridging Zn and Ga atoms E. In fact, with a partial Ga/Zn exchange, the molecular compounds $[Mo(GaMe)_4(ZnCp^*)_4]$, $[Mo(GaMe)_2(ZnMe)_4(ZnCp^*)_4]$, and $[Rh(GaMe)(ZnMe)_3(ZnCp^*)_4]$ were obtained as examples of the family of mononuclear, ternary M/Ga/Zn mixed compounds. Interestingly, all of these compounds feature no significant structural changes if the Ga/Zn ratio is altered, as was found for the related intermetallic solid-state compounds.[19] Structural relationships of the metal core units of these metal-rich molecules to Hume−Rothery solid-state phases are obvious in some cases. For example, the structural element of a Mo atom which is icosahedrally surrounded by 12 Zn atoms, e.g., the $MoZn_{12}$ core unit, is found in the bimetallic coordination compound $[Mo(ZnCp^*)_3(ZnMe)_9]$ as well as in the solid-state structure of $MoZn_{20.44}$.[18a] Furthermore, the larger, CO-protected congener $[\{Mo(CO)_4\}_4Zn_6(ZnCp^*)_4]$ exhibits a Zn_6 octahedron embedded in a Mo_4 tetrahedron, which is also found in $MoZn_{20.44}$.[18b] Likewise, the structural motifs of two superimposed M_4 and M'_4 tetrahedra are found in the molecular structures of the clusters $[Cu_4(CN\text{-}t\text{-}Bu)_4(ZnCp^*)_4]$[18c] and $[Cu_6(AlCp^*)_6H_4]$[18d] as well as the solid-state structure of γ-brass[20b] (Figure 1).

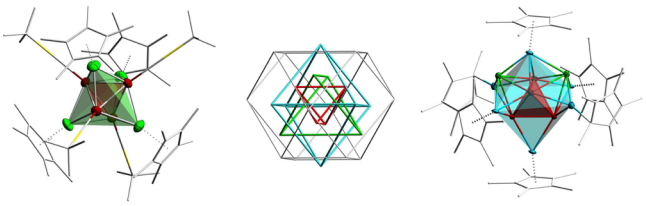

Figure 1. Molecular structures of $[Cu_4(CN\text{-}t\text{-}Bu)_4(ZnCp^*)_4]$ (left)[18c] and $[Cu_6(AlCp^*)_6H_4]$ (right)[18d] and a respective cutout of the solid-state structure of γ-brass (center).

The list of binuclear and oligonuclear molecular congeners of Hume−Rothery intermetallics is, however, short. The only binuclear example has so far been the all hydrocarbon-protected, 10-metal-atom ternary cluster $Pd_2Zn_6Ga_2$ of the formula $[Pd_2Zn_6Ga_2(Cp^*)_5(Me)_3]$.[21] Herein, we describe the discovery of new examples of the envisaged family of binuclear Hume−Rothery phase-inspired metal-rich molecules: the 10-metal-atom Ni_2Zn_7E clusters $[(\eta^5\text{-}Cp^*)Ni_2(ZnMe)_6(ZnCp^*)(ECp^*)]$ (**1-Zn**. E = Zn; **1-Ga**. E = Ga) and $[(\eta^6\text{-}$toluene$)Ni_2(ZnCp^*)_2(ZnMe)_6]$ (**2**). The compounds were obtained via Ga/Zn and Al/Zn exchange reactions from the starting materials $[Ni_2(ECp^*)_3(C_2H_4)_2]$ (E = Al, Ga; Scheme 1). We will show that these molecules can (conceptually) be viewed as metalloligand analogues of the 34 ve triple-decker cluster $[CpNiCpNiCp]^+$, known to organometallic and molecular cluster textbooks.

Scheme 1. Synthesis of 1-Zn and 1-Ga as well as 2

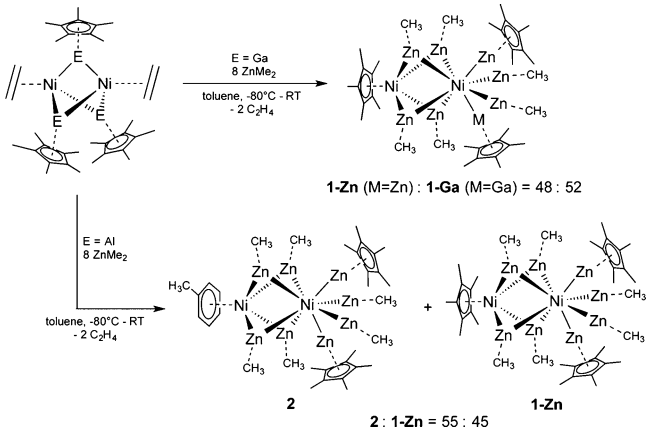

RESULTS AND DISCUSSION

1. Synthesis and Composition. Treatment of the binuclear complex $[Ni_2(GaCp^*)_3(\eta^2\text{-}C_2H_4)_2]$ with an 8-fold molar excess of a 1.2 M solution of $ZnMe_2$ in toluene at low temperature (−80 °C) leads to an immediate color change from light red to dark red during warmup to ambient temperature. After standard workup procedures (see the Experimental Section), well-shaped dark-red prismatic single crystals were collected in good yield around 42% (see Scheme 1). The analytically pure product, however, turned out to be a mixture of the two very closely related "Zn/Ga-substitution isomers" of the formula $[(\eta^5\text{-}Cp^*)Ni_2(ZnMe)_6(ZnCp^*)(ECp^*)]$ (**1-Zn**, E = Zn; **1-Ga**, E = Ga). Notably, Cp* transfer, which has been observed in former related reactions,[22] presumably from GaCp* onto Ni, occurred, and all ethylene ligands were liberated during the reaction. Because of very fast reaction with $ZnMe_2$ even at −80 °C, meaningful NMR reaction studies on the building process of **1-Zn** and **1-Ga** could not be performed. Higher reaction temperatures (>50 °C) and longer reaction times, in order to avoid residual Ga incorporation, failed, and in all of these experiments, the pseudohomoleptic mononuclear, all-Zn-coordinated compound $[Ni(ZnCp^*)_4(ZnMe)_4]$[19] was formed, as deduced from NMR studies. In order to avoid Ga incorporation from the very beginning, the Ga-free Ni_2Al_3 starting compound $[Ni_2(AlCp^*)_3(C_2H_4)_2]$* was used (which can be obtained from a ligand-exchange reaction of $[Ni_2(GaCp^*)_3(C_2H_4)_2]$ with AlCp*).[23] Employing the same reaction conditions as those for **1-Zn** and **1-Ga**, i.e., the treatment of $[Ni_2(AlCp^*)_3(C_2H_4)_2]$ with 8 equiv of a 1.2 M solution in toluene, another closely related, nevertheless slightly different, product mixture was isolated, and the compounds were characterized. This mixture consists of $[(\eta^6\text{-}$toluene$)Ni_2(ZnCp^*)_2(ZnMe)_6]$ (**2**) and, interestingly, again **1-Zn**. Both product mixtures, **1-Zn**/**1-Ga** and **2**/**1-Zn**, cannot be separated. The physical properties are too similar, such as their

dx.doi.org/10.1021/ic5014335 | Inorg. Chem. 2014, 53, 10403−10411

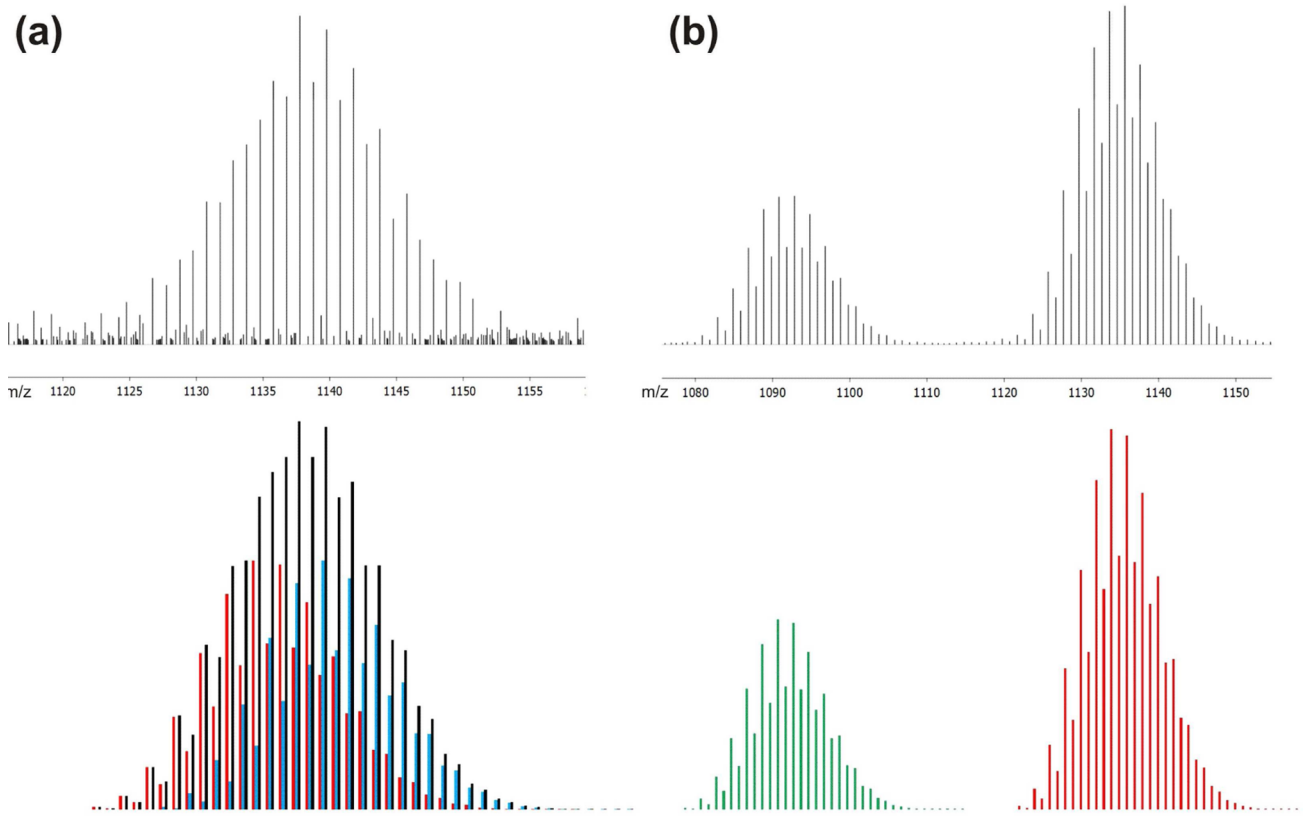

Figure 2. (Top) Experimental LIFDI MS spectra of the crystalline materials derived from the reaction of (a) $[Ni_2(GaCp^*)_3(C_2H_4)_2]$ with $ZnMe_2$ in toluene and (b) $[Ni_2(AlCp^*)_3(C_2H_4)_2]$ with $ZnMe_2$ in toluene. (Bottom) Calculated isotopic patterns of (a) a mixture of **1-Ga** and **1-Zn** (black), overlaid with the isotopic patterns of **1-Zn** (red) and **1-Ga** (blue) and (b) a 2:1 mixture of **1-Zn** (red) and **2** (green), respectively.

solubility in various solvents, and because of extreme sensitivity to moisture and air contact, the losses in repeated recrystallization experiments were too high. While the mixture **1-Zn**/**1-Ga** cocrystallizes, two different crystal types are obtained for **2** and **1-Zn**. Not surprisingly, but unfortunately, systematic manual separation of the single crystals under the microscope proved to be ineffective because both crystal types are too similar to be distinguished.

2. Analytical Characterization. *2.1. [(η^5-Cp*)-$Ni_2(ZnMe)_6$(ZnCp*)(ECp*)] (**1-Zn**, E = Zn; **1-Ga**, E = Ga).* ^{1}H NMR studies of a pure sample of **1** show the presence of two distinctly different products: Compound **1-Zn** gives rise to three broad resonances at 9.43 ppm (12H), 5.86 ppm (45H), and −10.9 ppm (6H) at room temperature, with the unusual chemical shifts and line widths underlining the paramagnetism of the sample (Figure S1 in the Supporting Information, SI). The assignment of the resonances cannot be performed unambiguously, but we suggest an overlap of the two chemically nonequivalent Cp* resonances, leading to a total integral ratio of 12:45:6. The ^{1}H NMR spectrum at −80 °C does not show splitting of the Cp* resonance; only a temperature-dependent chemical shift can be observed (see Figures S1 and S2 in the SI). The resonances for the diamagnetic **1-Ga** are found at 2.19 ppm (15H, ZnCp*), 2.11 ppm (15H, GaCp*), and 1.87 ppm (15H, NiCp*); i.e., three individual Cp* resonances can be observed together with two distinct ZnMe signals at 0.16 ppm (12H, μ_2-ZnMe) and 0.01 ppm (6H, ZnMe) at room temperature. Taking the solid-state structures (see below) of the molecule into account, these resonances can be clearly assigned if the Ga is assumed to be placed in the position of one of the two (symmetrically equivalent) terminal ECp* ligands, leaving four (equivalent) bridging and two (equivalent) terminal ZnMe ligands as well as one terminal ZnCp* ligand. ^{13}C NMR studies cannot be performed because of the very low stability of the samples in solution. The presence of a **1-Zn**/**1-Ga** mixture with a molar ratio of 0.48:0.52 (derived by NMR) of all-Zn-ligated (**1-Zn**) and Ga/Zn-mixed-ligated (**1-Ga**) compounds is further supported by liquid-injection field desorption ionization (LIFDI) mass spectrometric (MS) analysis, as depicted in Figure 1a. The isotopic pattern with alternating strong and weaker intensities, as well as the corresponding peaks of highest mass, for the calculated patterns of **1-Zn** (Figure 2a, bottom, blue trace) and **1-Ga** (Figure 2a, bottom, red trace) do not match with the experimentally measured isotopic pattern depicted in Figure 2. However, the calculated isotopic pattern of a mixture of both **1-Zn** and **1-Ga** in a ratio of 0.48:0.52 (Figure 2a, bottom, orange trace) yields a very pleasing match with the experimental data with an effective "molecular ion" peak $[M]^+$ of m/z 1138.8 for **1**.

*2.2. [(η^6-Toluene)$Ni_2(ZnCp^*)_2(ZnMe)_6$] (**2**).* The ^{1}H NMR spectrum of the product mixture **2**/**1-Zn**, as synthesized by the reaction described above, shows the presence of **1-Zn** by two broad resonances at 9.43 ppm (18H) and 5.86 ppm (45H) equal to those described above. The characteristic resonance for compound **2** can be found at 2.19 ppm (30H, ZnCp*) for the two chemically equivalent ZnCp* ligands. One single and very broad resonance at −0.04 ppm (18H) is observed for all (bridging and terminal) ZnMe units, indicating a fast fluxional exchange process at room temperature on the NMR time scale.

dx.doi.org/10.1021/ic5014335 | Inorg. Chem. 2014, 53, 10403−10411

The signals for the η^6-toluene ligand are found at 1.82 ppm (3H), 5.88 ppm (2H), 5.85 (2H), and 5.67 ppm (1H). ^{13}C NMR measurements are in good agreement with the idealized C_{4v} symmetry of the molecule in the solid-state structure (vide infra). The ^{13}C NMR resonances for **2** can be observed at 118.72, 110.26, 103.38, 100.89, and 2.13 ppm for the toluene ligand, as well as at 110.91 and 10.79 ppm for the Cp* units. No resonances of **1-Zn** were found because of the paramagnetic nature of the molecule. Similar to the above cases of **1-Zn** and **1-Ga**, the presence of a mixture of **1-Zn** and **2** is supported by LIFDI MS analysis, as depicted in Figure 1b. Now, the molar masses of the two compounds are significantly different, and the patterns do not overlap. Thus, each experimental isotopic pattern assigned to **1-Zn** and **2**, respectively, matches very nicely with the calculated ones. The measured molecular ion peaks $[M]^+$ (m/z 1093.3 and 1136.4) also match with the calculated values of m/z 1092.7 (**1-Zn**) and 1135.8 (**2**), respectively. From the MS data, a 1:2 molar ratio of **1-Zn** and **2** is derived, which does not fully match with the molar ratio of 1:1.27 derived by NMR resonance integration. This (small) discrepancy is assigned to some different ionization behavior and stability under high-vacuum conditions (different shell of ancillary hydrocarbon ligands).

3. Structural Characterization. *3.1. 1-Zn and 1-Ga.* The molecular structure of **1**, as determined by single-crystal X-ray diffraction (XRD), is depicted in Figure 3. The position of the Ga atom cannot be rigorously assigned on the basis of routine single-crystal XRD data. The assignment of the position was done on the basis of the ^{1}H NMR data of this compound (vide supra), assuming a rigid structure (i.e., no difference between the solution and solid state). Both Ni centers are surrounded by four different types of ligands, i.e., two terminal ECp* (E = Zn/Ga), two terminal ZnMe, four bridging ZnMe, and one Cp* ligand, resulting in an overall Ni_2Zn_7E core of 10 metal atoms wrapped in the hydrocarbon ligand shell (E = Zn, **1-Zn**; E = Ga, **1-Ga**). The overall symmetry of the metal core of **1-Zn** is C_{4v}, while in **1-Ga**, the highest symmetry is C_s with a mirror plane spanned through both Ni atoms and the Ga atom. The most similar Ni cluster found in the literature is the octahedral cluster $[Ni_2Zn_4Cp_6]$ with two apical NiCp centers bridged by four coplanar, basal ZnCp units.[24] The arrangement of metal atoms in **1** is best described as a singly capped square antiprism with the NiCp* fragment as the capping unit of one Zn_4 face. This is reflected by continuous-shape-method analysis (CShM)[25−27] with a value of $S_Q(P) = 1.25$, being sufficiently close to the ideal value of 1.0. In comparison, a tricapped-trigonal-prismatic or dodecahedral arrangement shows significantly higher CShM values (for details, see the SI). Some minor deviations from an ideal capped square antiprism arise because of four ZnMe units bridging both Ni atoms, indicating attractive interaction between the central Ni and the apical NiCp* fragment (see Figures S3 and S4 in the SI). The two ECp* groups are located in a trans position, similar to the T_d-symmetric ligand arrangement in the dodecahedral complex $[Ni(ZnCp^*)_4(ZnMe)_4]$. The Ni1−Zn-Me vector for the terminal ZnMe groups deviates from linearity (av. 158.4°). The MCp* units [M = Ni, Zn (Ga)] show all-η^5-coordination of the Cp* groups with only small deviations of the Ni1−M−Cp*$_{centroid}$ angles from the expected linearity (M = Ni2, 177.4°; Zn1, 176.1°; Zn2, 173.6°). In addition, the E−Cp*$_{centroid}$ distances (av. 1.93 Å) match nicely the reported distances of $[Ni(ZnCp^*)_4(ZnMe)_4]$ (av. 1.93 Å), and these distances are significantly shorter than those of $[Zn_2Cp^*_2]$ (av. 2.04 Å). The Ni−Cp*$_{centroid}$ distance of 1.752 Å is similar to that of the "piano-stool" complex $[Cp^*Ni(ZnCp^*)_3]$ (1.730 Å) and slightly shorter than that in nickelocene $Ni(C_5H_5)_2$ (1.817 Å).[17,28] The Ni1−Zn bond distances ("central" Ni) vary less than 1% with an average value of 2.367 Å and are significantly shorter than the Ni2−Zn distances (apical Ni) with an average value of 2.473 Å. Nevertheless, all Ni−Zn distances follow the trend Ni2−ZnMe$_{bridging}$ > Ni1−ZnMe$_{bridging}$ > Ni1−ECp* > Ni1−ZnMe$_{terminal}$. In summary, the related Ni−Zn distances of **1** are quite similar to those found in the series of other Zn-rich Ni clusters $[Ni(ZnCp^*)_4(ZnMe)_4]$ [2.351(1)−2.371(1) Å for Ni−ZnCp* and 2.313(1)−2.330(1) Å for Ni−ZnZnCp*], $[Ni(ZnCp^*)_4(ZnZnCp^*)_4]$[29] [2.351(1)−2.371(1) Å for Ni−ZnCp* and 2.313(1)−2.330(1) Å for Ni−ZnMe], or $[Ni_2Zn_4Cp_6]$[24] [2.398(2) Å, ranging from 2.352(1) to 2.520(1) Å]. All values are somewhat shorter than the average Ni−Zn distance found in the intermetallic phase Ni_1Zn_1 of the CsCl structure type (e.g., octacoordinated Ni; Ni−Zn, 2.525 Å).[30] The distances Zn−Zn of **1** are between 2.735 and 3.072 Å and match nicely with the Zn−Zn contacts found in the Ni_1Zn_1 intermetallic phase. Note that the γ-brass-type phase Ni_2Zn_{11} features a Ni−Zn distance of 2.611 Å.[31]

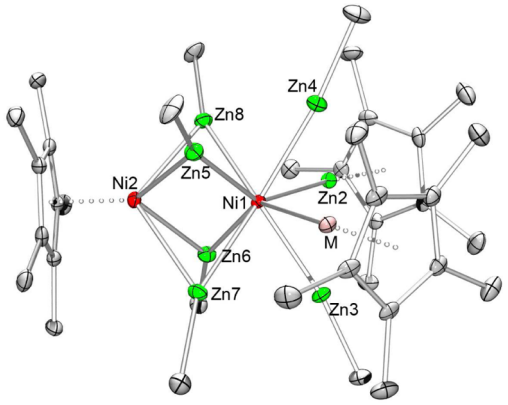

Figure 3. Povray plot of the molecular structure of **1** in the solid state as determined by single-crystal XRD (thermal ellipsoids are shown at the 50% probability level and H atoms as well as cocrystallized solvent molecules have been omitted for clarity). Selected bond length and distances (Å) as well as angles (deg): Ni1−Ni2 2.517(1), Ni1−M 2.366(1), Ni1−Zn2 2.361(1), Ni1−Zn3 2.340(1), Ni1−Zn4 2.352(1), Ni1−Zn5 2.384(1), Ni1−Zn6 2.372(1), Ni1−Zn7 2.374(1), Ni1−Zn8 2.386(1), Ni2−Zn5 2.520(1), Ni2−Zn6 2.432(1), Ni2−Zn7 2.431(1), Ni2−Zn8 2.511(1), Zn−Zn/M 2.735−3.072 (av. 2.89), Ni2−Cp*$_{centroid}$ 1.752, M−Cp*$_{centroid}$ 1.933, Zn2−Cp*$_{centroid}$ 1.931; Ni1−Zn3−Me 173.4(2), Ni1−Zn4−Me 171.3(2), Ni1−Zn5−Me 159.1(2), Ni1−Zn6−Me 158.1(2), Ni1−Zn7−Me 157.8(2), Ni1−Zn8−Me 158.7(2), Ni2−Zn5−Me 138.8(2), Ni2−Zn6−Me 138.0(2), Ni2−Zn7−Me 138.7(2), Ni2−Zn8−Me 139.3(2), Cp*$_{centroid}$−Ni2−Ni1 177.44, Cp*$_{centroid}$−M−Ni1 173.62, Cp*$_{centroid}$−Zn2−Ni1 176.11.

3.2. Compound 2. The molecular structure of **2** (Figure 4) is very similar to that of **1-Zn**. A detailed discussion will be omitted. The Ni_2Zn_8 core can be described as a capped square antiprism [$S_Q(P)$ value of 1.30; see Table S1 in the SI]. The direct comparison of **2** and **1-Zn** gives a $S_Q(P)$ value of 0.16, further underlining the structural similarity of the two compounds (see Figures S3 and S4 in the SI).

The structurally most interesting feature of **2** with respect to **1** is the toluene molecule coordinated to Ni2. The Ni−toluene$_{centroid}$ distance of **2** is 1.635 Å, which is rather similar to those other nickel(0) arene complexes found in the literature:

dx.doi.org/10.1021/ic5014335 | Inorg. Chem. 2014, 53, 10403−10411

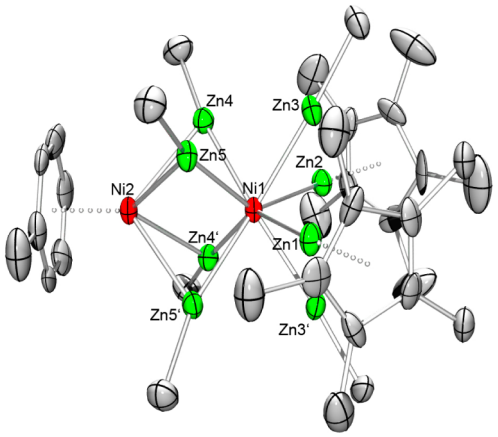

Figure 4. Povray plot of the molecular structure of **2** in the solid state as determined by single-crystal XRD (crystallographic equivalent atoms are generated by a mirror plane (Ni2, Zn1, Ni1, and Zn2), thermal ellipsoids are shown at the 50% probability level, and H atoms have been omitted for clarity). Selected bond length and distances (Å) as well as angles (deg): Ni1−Ni2 2.615(2), Ni1−Zn1 2.365(2), Ni1−Zn2 2.358(2), Ni1−Zn3 2.347(1), Ni1−Zn4 2.365(1), Ni1−Zn5 2.364(1), Ni2−Zn4 2.505(1), Ni2−Zn5 2.533(1), Zn−Zn 2.793−2.947 (av. = 2.873), Ni2−toluene$_{centroid}$ 1.635, Zn1−Cp*$_{centroid}$ 1.946, Zn2−Cp*$_{centroid}$ 1.946; Ni1−Zn3−Me 176.2(2), Ni1−Zn4−Me 164.8(3), Ni1−Zn5−Me 169.3(3), Ni2−Zn4−Me 130.2(3), Ni2−Zn5−Me 124.5(3), toluene$_{centroid}$−Ni2−Ni1 177.28, Cp*$_{centroid}$−Zn1−Ni1 174.60, Cp*$_{centroid}$−Zn2−Ni1 175.48.

[{(μ_2-η^6-IPr)Ni}$_2$][9] [IPr = 1,3-bis(2,6-diisopropylphenyl)-imidazol-2-ylidene; Ni-[η^6-C_6H_3(*i*-Pr)$_2$]$_{centroid}$ = 1.607 Å], [$C_3H(CH_2)(CH_3)(C_6H_3$-2,6-*i*-$Pr_2)_2$)SiNi(η^6-toluene)][10] [Ni−(η^6-toluene)$_{centroid}$ = 1.592 Å], [(η^1-*t*-Bu_2PCH_2P-*t*-Bu_2)Ni(η^6-benzene)][8] [Ni−(η^6-benzene)$_{centroid}$ = 1.619 Å], [(R^H_2Si)Ni-(η^6-toluene)][11] [R^H = 1,1,4,4-tetrakis(trimethylsilyl)butane-1,4-diyl; Ni−(η^6-toluene)$_{centroid}$ = 1.618 Å], and [Ni_2(GaAr′)$_2$(η^1:η^1-μ_2-C_2H_4)][12] [Ar′ = C_6H_3-2,6-(C_6H_3-2,6-*i*-Pr_2)$_2$; Ni−(η^6-C_6H_3-2,6-*i*-Pr_2)$_{centroid}$ = 1.679 and 1.672 Å]. The Ni1−Zn and Zn−Zn distances in **2** are very similar to those of compound **1**, and likewise the trend for the Ni−Zn distances is Ni2−ZnMe$_{bridging}$ ≥ Ni1−ZnMe$_{bridging}$ > Ni1−ZnCp* > Ni1−ZnMe$_{terminal}$. A small but significant difference is found in the Ni−Ni distance, which is somewhat longer in **2** [2.615(2) Å] than in **1** [2.517(1) Å]. At this point of our discussion, we emphasize that compounds **1** and **2** can be viewed as metallo analogues of the well-known textbook example of a Ni triple-decker cluster cation, [(η^5-C_5H_5)$_3Ni_2$]$^+$, which exhibits a valence-electron (ve) count of 34; the same is obtained for **2**. Each of the eight ZnR units (R = Me, Cp*) contributes one electron, the toluene ligand contributes six, and both Ni atoms (d^{10}) contribute a total of 20 electrons, which sums up to 34. Both compounds **1** and **2** can be divided into two parts, i.e., the electronically saturated 18 ve moiety [Ni(ZnR)$_8$] and the electrophilic fragments 15 ve NiCp* or 16 ve Ni(η^6-toluene), respectively. A similar reasoning has been made for [$Pd_2Zn_6Ga_2Cp^*_5Me_3$].[21] In order to obtain more detailed insight into the bonding situation of **1** and **2**, we have performed theoretical analysis on the level of DFT (see section 4).

4. Physical Properties, Electron Paramagnetic Resonance (EPR), and Cyclic Voltammetry (CV) Measurements. In contrast to **1-Ga** (34 ve), which is diamagnetic, **1-Zn** (33 ve) is paramagnetic. The EPR spectrum of the product mixture **2** indeed shows a sharp anisotropic signal at 3203.0 G for **1-Zn**, with *g* values of g_1 = 2.388, g_2 = 2.115, and g_3 = 2.016 (see Figure 5, top). However, the product mixture **1**, which also

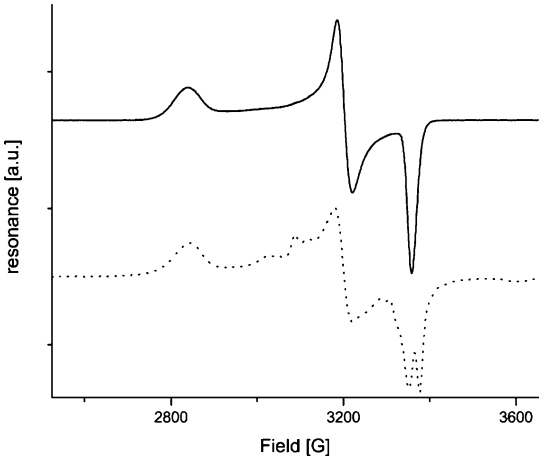

Figure 5. EPR spectra of product mixtures (top) **1-Zn**/**2** and (bottom) **1-Zn**/**1-Ga** (toluene, 50 K).

contains **1-Zn**, reveals additional signals in the same region, which might indicate decomposition due to the low stability of **1** in solution. The extraction of *g* values was impossible because of overlap of the signals; also several attempts to subtract the spectra of **1** and **2** did not give conclusive results.

Furthermore, CV studies were performed that show no significant redox-active processes but rather a fast decomposition, confirming the low stability of the compounds (see the SI). The solutions turned brown shortly after the beginning of the experiment, higher concentrations, various step widths, and different conducting salts and potentials did not give different results.

5. Theoretical Characterization of the Bonding Situations. We optimized the geometries of **1-Zn**, **1-Ga**, and **2** with DFT calculations at the BP86/TZVPP level, and we analyzed the bonding situation with quantum-chemical methods. The calculated bond lengths of the Zn species **1-Zn** agree better with the results of the X-ray refinement of **1** than the theoretical data of **1-Ga** (Table S3 in the SI). This holds in particular for the Ni1−Ni2 distance, where the calculated value for **1-Ga** is much longer than the experimental data. Further support comes from the calculated data for the Ni1−Ga, Ni2−Zn5, and Ni2−Zn8 distances, which are significantly longer than the measured values of **1**. Metal−ligand distances of transition-metal complexes tend to become shorter in the solid state compared with the free molecules because of intermolecular interactions. The calculated data for **2** agree quite well with the experimental results, where the theoretical Ni−Ga distances are always slightly too long (Table S4 in the SI).

Compound **1-Zn** is formally a 33 ve complex in the electronic doublet state, which has one unpaired electron. Figure 6 shows that the unpaired electron is mainly localized at the Ni atom of NiCp*, which confirms that **1-Zn** can be discussed in terms of interactions between a closed-shell 18 ve complex interacting with open-shell 15 ve fragment NiCp*.

Detailed insight into the bonding situation of **1-Zn**, **1-Ga**, and **2** is given by the results of the EDA-NOCV calculations, which are presented in Table 1. The calculations were carried out using various fragments, as given in the first line of the table

dx.doi.org/10.1021/ic5014335 | *Inorg. Chem.* 2014, 53, 10403−10411

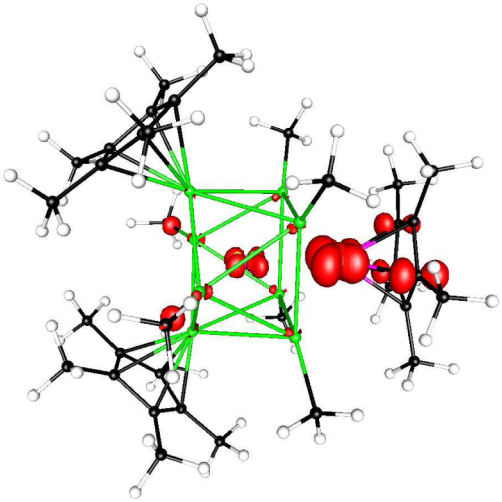

Figure 6. Visualization of the excess α-spin density of **1-Zn** (BP86/def2-TZVPP). The chosen contour value is 0.005.

and the remaining moieties. The interaction energies ΔE_{int} suggest that the bonding between the NiCp* fragment and the remaining part of the complex is stronger than the bonding of the metal fragments ZnCp* and ZnMe and that the bonding of NiCp* has a much higher electrostatic character than those of the other fragments. The bonding of NiCp* becomes even stronger in **1-Ga**, while the other fragments are slightly weaker bonded (Table 2). It is remarkable that the GaCp* species is significantly weaker bonded than the other fragments. The calculations indicate that the four moieties ZnCp*, $ZnMe_{terminal}$, $ZnMe_{bridging}$, and Ni(η^6-toluene) have bond strengths nearly identical with those of the remaining fragments.

Further insight into the electronic structure of the molecules comes from the QTAIM calculations of **1-Zn**, **1-Ga**, and **2**. Figure 6 shows the Laplacian distribution $\nabla^2\rho(r)$ and the bond paths and zero-flux surfaces of **1-Zn** in two different planes. The most important information comes from the bond paths, which suggest that there is a Ni1−Ni2 binding interaction. The bridging Zn atoms have bond paths to both Ni atoms (Figure 7), while the terminal Zn atoms have only one bond path. The Laplacian distributions for **1-Ga** and **2**, which are shown in the SI, exhibit similar features, i.e., bond paths for Ni1−Ni2, bond paths of the Zn atoms to both Ni atoms, and the only bond path between the terminal Zn or Ga atoms to Ni1.

CONCLUSION

We have presented the synthesis, spectroscopic and structural characterization as well as theoretical investigations on the bonding situation of three new examples of the molecular Zn/Ga/Ni clusters **1-Zn** and **1-Ga** and **2**. Unfortunately, we were not able to isolate each of the identified new molecules in pure form but rather characterized them as a mixture of **1-Zn** together with **1-Ga** or **1-Zn** with **2**. Similar to Zn-rich intermetallic phases, the transition metals (here Ni) are distributed in a matrix of Zn atoms to yield highly Zn-coordinated environments (here octacoordination of one Ni). The organic residues, the ancillary ligands Me, Cp*, and toluene, can be viewed as a "protecting" shell of the 10-metal-atom core structures of the title compounds. It is important to realize that this particular choice of stabilizing organic substituents is not at all arbitrary or could be replaced by a wider variety of other ligands. The soft and flexible binding properties of Cp* and the transferability of Me between groups 12 and 13 are essential for the success of this precedence-less type of cluster formation reaction. The organo Zn substituents serve as suitable ligands for stabilization of the less-common Ni(η^6-arene) and the common Ni(η^5-Cp*) fragments, or the other way around, Ni(η^6-arene) and Ni(η^5-Cp*) moieties serve as good candidates for the trapping of reactive fragments $[Ni(ZnR)_a(GaR)_b]$ ($a + 2b = 8$, where $b \leq 1$). Further experiments with NiCp* transfer reagents like $[NiCp^*_2]$ or $[Ni_2Cp^*_3]^+$ (also the respective Cp derivatives) are under current investigation. However, our preliminary results showed that products are so far too unstable under the reaction conditions to be isolated and purified.

Formation of the new clusters is conceptually addressed as cluster expansion (Zn_4 face capping) of the so far not selectively accessible species $[Ni(ZnMe)_6(ZnCp^*)_2]$. Rather, we have the more shielded tetra-Cp*-substituted $[Ni(ZnMe)_4(ZnCp^*)_4]$ in our hands. As mentioned above, it turned out in our experiments that this compound does not easily add NiCp* fragments. Obviously, more delicate steric

Table 1. EDA-NOCV Results (BP86/TZ2P+) for 1-Zn, 1-Ga, and 2 Using Various Fragments[a]

fragment A[d]	ZnCp*	GaCp*	$ZnMe_{terminal}$	$ZnMe_{bridging}$	NiCp*
			1-Zn		
ΔE_{int}	−76.5		−58.3	−66.0	−82.6
ΔE_{Pauli}	241.5		211.3	280.1	207.0
ΔE_{elstat}[b]	−176.9 (55.6%)		−160.2 (59.4%)	−198.7 (57.4%)	−203.4 (70.2%)
ΔE_{orb}[b]	−141.2 (44.4%)		−109.5 (40.6%)	−147.5 (42.6%)	−86.3 (29.8%)
			1-Ga		
ΔE_{int}	−67.8	−33.7	−58.1	−64.3	−114.4
ΔE_{Pauli}	169.8	162.7	203.7	293.0	240.7
ΔE_{elstat}[b]	−151.5 (63.8%)	−126.5 (64.4%)	−162.7 (62.2%)	−206.3 (57.7%)	−226.2 (63.7%)
ΔE_{orb}[b]	−86.1 (36.2%)	−69.9 (35.6%)	−99.0 (37.8%)	−151.0 (42.3%)	−128.9 (36.3%)
			2		
ΔE_{int}	−69.8		−65.5	−69.7	−69.9[c]
ΔE_{Pauli}	165.1		206.7	268.6	176.5[c]
ΔE_{elstat}[b]	−151.7 (64.6%)		−167.8 (61.6%)	−201.9 (59.7%)	−176.2 (71.5%)[c]
ΔE_{orb}[b]	−83.1 (35.4%)		−104.4 (38.4%)	−136.4 (40.3%)	−70.2 (28.5%)[c]

[a]Energy values are given in kcal/mol. [b]The percentage values in parentheses give the attractive contribution to ΔE_{int}. [c]The fragment is Ni(toluene). [d]Fragment B is the rest of the molecule.

dx.doi.org/10.1021/ic5014335 | Inorg. Chem. 2014, 53, 10403−10411

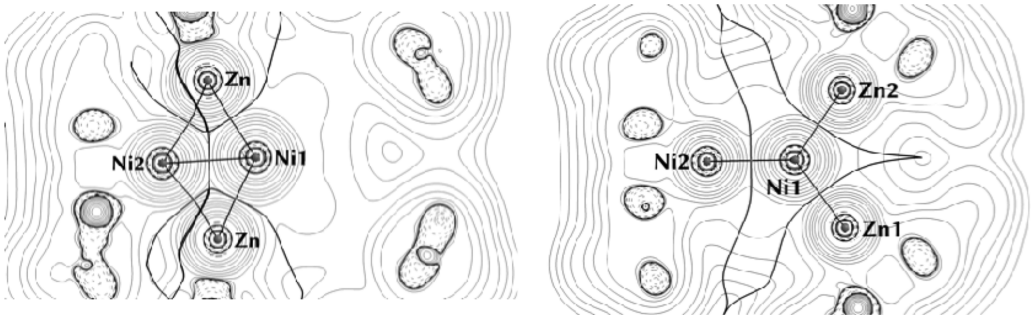

Figure 7. Contour line diagrams $\nabla^2\rho(r)$ of the complex **1-Zn**. The solid lines indicate areas of charge concentration $[\nabla^2\rho(r) < 0]$, while dashed lines show areas of charge depletion $[\nabla^2\rho(r) > 0]$. The thick solid lines connecting the atomic nuclei are the bond paths. The thick solid lines separating the atomic basins indicate the zero-flux surfaces crossing the molecular plane.

and kinetic factors are important, and the outcome of the respective reactions is controlled by the availability of appropriate starting compounds as building blocks. Quite interestingly, we observe for the first time open-shell molecules, such as the compound **1-Zn**, in contrast to the family of mononuclear Zn-rich molecules, which strictly follow the closed-shell 18 ve counting. However, the obtained new "dinuclear" Ni compounds match the cluster valence-electron rules known from classic organometallic (metallocene-type) clusters. To us, this is a very significant discovery. It gives a hint that systematic cluster expansion is possible in this Hume–Rothery-inspired organometallic chemistry and even larger aggregates could be obtained. Known cluster valence-electron counting rules may be applied to guide the synthesis.

EXPERIMENTAL SECTION

General Remarks. All manipulations were carried out in an atmosphere of purified argon using standard Schlenk and glovebox techniques. Hexane, toluene, and tetrahydrofuran were dried using a MBraun Solvent Purification System. The final H_2O content in all solvents was checked by Karl Fischer titration and did not exceed 5 ppm. $[Ni_2(GaCp^*)_3(C_2H_4)_2]$ and $[Ni_2(AlCp^*)_3(C_2H_4)_2]$[23] were prepared according to recent literature methods. Elemental analyses were performed by the microanalytical laboratory at the Ruhr University Bochum. NMR spectra were recorded on a Bruker Avance DPX-250 spectrometer (^{1}H, 250.1 MHz; ^{13}C, 62.9 MHz) in either C_6D_6 or C_7H_8 at various temperatures of 228 to 378 K. Chemical shifts are given relative to tetramethylsilane (TMS) and were referenced to the solvent resonances as internal standards. The chemical shifts are described in parts per million (ppm), are downfield-shifted from TMS, and are consecutively reported as position (^{1}H and ^{13}C), relative integral, multiplicity (s = singlet, m = multiplet), coupling constant (J in Hz), and assignment. MS was measured with a Jeol AccuTOF GCv and Waters LCT: ionization method, liquid-injection field desorption ionization (LIFDI); the special ionization cell was obtained from Linden CMS GmbH, Leeste, Germany (http://www.linden-cms.de). ESR spectra were recorded with a Bruker-Elexsys E500 ESR spectrometer with an ER077R magnet (75 mm gap between pole faces), an ER047 XG-T microwave bridge, and an ER4102ST resonator with a TE_{102} cavity.

Crystallography. The XRD intensities from the crystals of compounds **1** and **2** were collected on an Oxford Xcalibur2 diffractometer with Mo Kα radiation (λ = 0.71073 Å) and a Sapphire2 CCD. The molecular structures were solved by direct methods using *SHELXS-97* and refined against F^2 on all data by full-matrix least squares with *SHELXL-97*.[32,33] The crystals were picked up with a glass fiber, coated with a perfluoropolyether, and immediately mounted in a cooled nitrogen stream of the diffractometer. Severely disordered cocrystallized toluene molecules were found in compound **1**, which could not be modeled properly, and its contributions were removed from the diffraction data with *PLATON/SQUEEZE*.[34,35] CCDC 968397 (**1**) and 968398 (**2**) contain the supplementary crystallographic data for this paper. These data can be obtained free of charge from the Cambridge Crystallographic Data Centre via www.ccdc.ac.uk/data_request/cif.

Computational Details. The geometries of the molecules were optimized at the gradient-corrected DFT level of theory using Becke's exchange functional[36] in conjunction with Perdew's correlation functional[37] (BP86) with the *TURBOMOLE V6.3.1* program package.[38] Ahlrich's def2-TZVPP basis set[39] was used. The RI approximation[40] was applied using auxiliary basis functions.[41] Stationary points were characterized by the analytical calculation of the Hessian using *TURBOMOLE*'s aoforce module.[42] This level of theory is denoted as BP86/def2-TZVPP. The QTAIM analyses were carried out with the program package *AIMAll*[43] at BP86/def2-TZVPP.

The EDA-NOCV calculations were carried out using the *ADF2012.01*[44] program package at the BP86/TZ2P+ level of theory. Uncontracted Slater-type orbitals (STOs) were employed as basis functions in self-consistent-field (SCF) calculations.[45] Triple-ζ-quality basis sets were used, which were augmented by two sets of polarization functions, that is, p and d functions for the H atom and d and f functions for the other atoms. An auxiliary set of s, p, d, f, and g STOs was used to fit the molecular densities and to represent the Coulomb and exchange potentials accurately in each SCF cycle.[46] Scalar relativistic effects were considered using the zero-order regular approximation.[47]

$[(\eta^5$-Cp)$Ni_2(ZnMe)_6(ZnCp^*)(ECp^*)]$ (**1**; **1-Zn**, E = Zn; **1-Ga**, E = Ga).* A solution of $[Ni_2(GaCp^*)_3(C_2H_4)_2]$ (150 mg, 0.190 mmol) in toluene (5 mL) was treated at −80 °C with a 1.2 M solution of $ZnMe_2$ (8 equiv, 1.27 mL, 1.52 mmol) in toluene. After the solution was warmed to room temperature within 10 min, a slight metal precipitate was observed. All volatile materials were evaporated in vacuo, and the residue was extracted with a small amount of toluene. Single crystals were obtained by cooling the extract solution to −30 °C for a few days. Yield: 90 mg (42%, dependent on Ni and 55% dependent on Zn/Ga) of a 1:1.07 mixture of **1-Zn** and **1-Ga**. **1-Zn**. ^{1}H NMR (250.1 MHz, C_6D_6, 297 K): δ 9.42 (br, 12H, μ_2-ZnMe), 5.86 (br, 45H, ZnCp*, NiCp*) −10.9 (br, 6H, ZnMe). **1-Ga**. ^{1}H NMR (250.1 MHz, C_6D_6, 297 K): δ 2.19 (s, 15H, ZnCp*), 2.11 (s, 15H, GaCp*), 1.87 (s, 15H, NiCp*), 0.16 (s, 12H, μ_2-ZnMe), 0.01 (s, 6H, ZnMe). No ^{13}C NMR data could be collected because of the very low stability of **1** in solution. Elem anal. Calcd for $C_{36}H_{63}Ni_2Zn_{7.5}Ga_{0.5}$: C, 37.9; H, 5.6; Zn, 43.1; Ga, 3.1. Found: C, 37.4; H, 5.5; Zn, 43.6; Ga, 2.7.

*$[(\eta^6$-Toluene)$Ni_2(ZnCp^*)_2(ZnMe)_6]$ (**2**).* The reaction procedure was similar to that of **1**, but instead $[Ni_2(AlCp^*)_3(C_2H_4)_2]$ (100 mg, 0.151 mmol) was used as the starting material. Yield: 82 mg (48%, dependent on Ni) of a 1:1.27 mixture of **2** and **1-Zn**. **2**. ^{1}H NMR (400.13 MHz, C_7D_8, 193 K): δ 5.67 (t, J = 6.0 Hz, 2H), 5.58−5.51 (d, J = 5.9 Hz, 2H), 5.41−5.30 (t, J = 5.6 Hz, 1H), 2.28 (s, 30H, ZnCp*), 1.72 (s, 3H, toluene), 0.25 (s, 12H, μ_2-ZnMe), 0.08 (s, 6H, ZnMe). **1-Zn**. ^{1}H NMR (400.13 MHz, C_7D_8, 193 K): δ 16.1 (br, 18H), 8.35 (br, 45H), −18.8 (br, 6H). ^{13}C NMR (100.6 MHz, C_6D_6, 297 K): δ 118.7, 110.9, 110.3, 103.4, 100.9, 10.9, 2.13. Elem anal. Calcd for

dx.doi.org/10.1021/ic5014335 | *Inorg. Chem.* 2014, 53, 10403−10411

$C_{33}H_{56}Ni_2Zn_8$: C, 36.25; H, 5.16; Zn, 47.9. Found: C, 37.0; H, 5.2; Zn, 46.3.

■ ASSOCIATED CONTENT

Supporting Information

X-ray crystallographic data in CIF format, NMR spectra of **1-Zn** and **2**, CShM measurements for the metal polyhedra of the molecular structures of **1** and **2**, experimental and analytical details for synthesis of the starting complexes $[Ni_2(GaCp^*)_3(\eta^2\text{-}C_2H_4)_2]$ and $[Ni_2(AlCp^*)_3(\eta^2\text{-}C_2H_4)_2]$, and crystallographic and computational details. This material is available free of charge via the Internet at http://pubs.acs.org.

■ AUTHOR INFORMATION

Corresponding Author

*E-mail: roland.fischer@ruhr-uni-bochum.de. Fax: (+49)234 321 4174.

Notes

The authors declare no competing financial interest.

■ ACKNOWLEDGMENTS

The dissertation project of MM was supported by the German Chemical Industry Fund (fellowship), the Ruhr University Research School (http://www.research-school.rub.de), and the German Research Foundation (Grant DFG Fi 502/23-2). The authors thank Linden CMS GmbH, Weyhe, Germany, and S. Bendix (Ruhr University Bochum) for support in MS, as well as Stefan Henke and Dr. Dirk Grothe (Organic Chemistry II, Ruhr University Bochum) for EPR measurements.

■ REFERENCES

(1) Kealy, T. J.; Pauson, P. L. *Nature* **1951**, *168*, 1039−1040.
(2) Wilkinson, G.; Rosenblum, M.; Whiting, M. C.; Woodward, R. B. *J. Am. Chem. Soc.* **1952**, *74*, 2125−2126.
(3) Fischer, E. O.; Pfab, W. *Z. Natuforsch.* **1952**, *7b*, 377−379.
(4) Miller, S. A.; Tebboth, J. A.; Tremaine, J. F. *J. Chem. Soc.* **1952**, 632−635.
(5) Weiss, E.; Fischer, E. O. *Z. Anorg. Allg. Chem.* **1956**, *286*, 142−145.
(6) Streitwieser, A., Jr.; Muller-Westerhoff, U.; Sonnichsen, G.; Mares, F.; Morrell, D. G.; Hodgson, K. O.; Harmon, C. A. *J. Am. Chem. Soc.* **1973**, *95*, 8644.
(7) Streitwieser, A., Jr.; Mueller-Westerhoff, U. *J. Am. Chem. Soc.* **1968**, *90*, 7364.
(8) Nickel, T.; Goddard, R.; Krüger, C.; Pörschke, K.-R. *Angew. Chem.* **1994**, *106*, 908−910.
(9) Lee, C. H.; Laitar, D. S.; Mueller, P.; Sadighi, J. P. *J. Am. Chem. Soc.* **2007**, *129*, 13802−13803.
(10) Meltzer, A.; Präsang, C.; Milsmann, C.; Driess, M. *Angew. Chem., Int. Ed.* **2009**, *48*, 3170−3173.
(11) Watanabe, C.; Inagawa, Y.; Iwamoto, T.; Kira, M. *Dalton Trans.* **2010**, *39*, 9414−9420.
(12) Serrano, O.; Hoppe, E.; Fettinger, J. C.; Power, P. P. *J. Organomet. Chem.* **2011**, *696*, 2217−2219.
(13) Grirrane, A.; Resa, I.; Rodriguez, A.; Carmona, E.; Alvarez, E.; Gutierrez-Puebla, E.; Monge, A.; Galindo, A.; Del Rio, D.; Andersen, R. A. *J. Am. Chem. Soc.* **2007**, *129*, 693−703.
(14) Resa, I.; Carmona, E.; Gutierrez-Puebla, E.; Monge, A. *Science* **2004**, *306*, 411.
(15) Bollermann, T.; Freitag, K.; Gemel, C.; Seidel, R. W.; von Hopffgarten, M.; Frenking, G.; Fischer, R. A. *Angew. Chem.* **2011**, *123*, 798−802.
(16) Bollermann, T.; Freitag, K.; Gemel, C.; Molon, M.; Seidel, R. W.; von Hopffgarten, M.; Jerabek, P.; Frenking, G.; Fischer, R. A. *Inorg. Chem.* **2011**, *50*, 10486−10492.
(17) Bollermann, T.; Freitag, K.; Gemel, C.; Seidel, R. W.; Fischer, R. A. *Organometallics* **2011**, *30*, 4123−4127.
(18) (a) Cadenbach, T.; Bollermann, T.; Gemel, C.; Fernandez, I.; von Hopffgarten, M.; Frenking, G.; Fischer, R. A. *Angew. Chem., Int. Ed.* **2008**, *47*, 9150−9154. (b) Cadenbach, T.; Gemel, C.; Fischer, R. A. *Angew. Chem., Int. Ed.* **2008**, *47*, 9146−9149. (c) Freitag, K.; Banh, H.; Gemel, C.; Seidel, R. W.; Kahlal, S.; Saillard, J.-Y.; Fischer, R. A. *Chem. Commun.* **2014**, *50*, 8681−8684. (d) Ganesamoorthy, C.; Wessing, J.; Kroll, C.; Seidel, R. W.; Gemel, C.; Fischer, R. A. *Angew. Chem., Int. Ed.* **2014**, *53*, 7943−7947.
(19) Cadenbach, T.; Bollermann, T.; Gemel, C.; Tombul, M.; Fernandez, I.; van Hopffgarten, M.; Frenking, G.; Fischer, R. A. *J. Am. Chem. Soc.* **2009**, *131*, 16063−16077.
(20) (a) Mizutani, U. *Hume−Rothery Rules for Structural Complex Alloy Phases*; CRC Press, Taylor & Francis: London, 2011. (b) Gourdon, O.; Gout, D.; Williams, D. J.; Proffen, T.; Hobbs, S.; Miller, G. J. *Inorg. Chem.* **2007**, *46*, 251−260.
(21) Bollermann, T.; Molon, M.; Gemel, C.; Freitag, K.; Seidel, R. W.; von Hopffgarten, M.; Jerabek, P.; Frenking, G.; Fischer, R. A. *Chem.—Eur. J.* **2012**, *18*, 4909−4915.
(22) Bollermann, T.; Puls, A.; Gemel, C.; Cadenbach, T.; Fischer, R. A. *Dalton Trans.* **2009**, 1372−1377.
(23) Steinke, T. Dissertation, Ruhr-Universität Bochum, Bochum, Germany, 2005. The preparative and analytical details for the two compounds are available in the SI file.
(24) Budzelaar, P. H. M.; Boersma, J.; Van der Kerk, G. J. M.; Spek, A. L.; Duisenberg, A. J. M. *Organometallics* **1985**, *4*, 680−683.
(25) Cirera, J.; Ruiz, E.; Alvarez, S. *Organometallics* **2005**, *24*, 1556−1562.
(26) Zabrodsky, H.; Peleg, S.; Avnir, D. *J. Am. Chem. Soc.* **1993**, *115*, 8278−8289.
(27) Molon, M.; Gemel, C.; von Hopffgarten, M.; Frenking, G.; Fischer, R. A. *Inorg. Chem.* **2011**, *50*, 12296−12302.
(28) Seiler, P.; Dunitz, J. D. *Acta Crystallogr., Sect. B* **1980**, *36*, 2255−2260.
(29) Bollermann, T. Dissertation, Ruhr University Bochum, Bochum, Germany, 2012.
(30) Heike, W.; Schramm, J.; Vaupel, O. *Metallwirtsch. Metallwiss. Metalltech.* **1936**, *15*, 655−662.
(31) Malik, Z.; Kneidinger, F.; Michor, H.; Puchegger, S.; Bauer, E.; Giester, G.; Rogl, P. *Intermetallics* **2013**, *38*, 88−91.
(32) Hübschle, C. B.; Sheldrick, G. M.; Dittrich, B. *J. Appl. Crystallogr.* **2011**, *44*, 1281−1284.
(33) Sheldrick, G. M. *SHELXL-97, Program for refinement of crystal structures*; University of Göttingen: Göttingen, Germany, 1997.
(34) Sluis, P. v. d.; Spek, A. L. *Acta Crystallogr.* **1990**, 46.
(35) Spek, A. L. *J. Appl. Crystallogr.* **2003**, *36*, 7−13.
(36) Becke, A. D. *Phys. Rev. A* **1988**, *38*, 3098.
(37) Perdew, J. P. *Phys. Rev. B* **1986**, *33*, 8822.
(38) Ahlrichs, R.; Bär, M.; Häser, M.; Horn, H.; Kölmel, C. *Chem. Phys. Lett.* **1989**, *162*, 165.
(39) Weigend, F.; Ahlrichs, R. *Phys. Chem. Chem. Phys.* **2005**, *7*, 3297.
(40) Ahlrichs, R. *Phys. Chem. Chem. Phys.* **2004**, *6*, 5119.
(41) (a) Eichkorn, K.; Treutler, O.; Häser, M.; Ahlrichs, R. *Chem. Phys. Lett.* **1995**, *242*, 652. (b) Eichkorn, K.; Weigend, F.; Treutler, O.; Ahlrichs, R. *Theor. Chem. Acc.* **1997**, *97*, 119. (c) Weigend, F. *Phys. Chem. Chem. Phys.* **2006**, *8*, 1057.
(42) Deglmann, P.; May, K.; Furche, F.; Ahlrichs, R. *Chem. Phys. Lett.* **2004**, *384*, 103.
(43) *AIMAll*: http://aim.tkgristmill.com. Last accessed: May 19, 2014.
(44) *ADF2012.01, SCM, Theoretical Chemistry*, Vrije Universiteit: Amsterdam, The Netherlands, http://www.scm.com. Last accessed: May 19, 2014.
(45) Snijders, J. G.; Vernooijs, P.; Baerends, E. J. *At. Data Nucl. Data Tables* **1981**, *26*, 483−509.
(46) Krijn, J.; Baerends, E. J. *Internal Report: Fit Functions in the HFSMethod*; Vrije Universiteit: Amsterdam, The Netherlands, 1984.

(47) (a) Chang, C.; Pelissier, M.; Durand, P. *Phys. Scr.* **1986**, *34*, 394−404. (b) Heully, J.-L.; Lindgren, I.; Lindroth, E.; Lundqvist, S.; Martensson-Pendrill, A.-M. *J. Phys. B* **1986**, *19*, 2799. (c) Snijders, J. *Chem. Phys. Lett.* **1996**, *252*, 51−61. (d) Lenthe, E. V.; Baerends, E. J.; Snijders, J. G. *J. Chem. Phys.* **1993**, *99*, 4597. (e) van Lenthe, E.; van Leeuwen, R.; Baerends, E. J.; Snijders, J. G. *Int. J. Quantum Chem.* **1996**, *57*, 281−293.